Astron. Astrophys. 57, 199—209 (1977)

ASTRONOMY AND ASTROPHYSICS

Acoustic Waves in the Solar Atmosphere

III. A Theoretical Temperature Minimum

P. Ulmschneider[1] and W. Kalkofen[2]

[1] Institut für Astrophysik, Am Hubland, D-8700 Würzburg, Federal Republic of Germany
[2] Center for Astrophysics, 60 Garden St., Cambridge, Mass. 02138 (USA)

Received July 19, revised October 29, 1976

Summary. In this third of a series of papers studying large amplitude acoustic waves we use the methods developed in previous papers to compute the propagation of acoustic waves until shock formation. A perturbation approach is used to let the waves travel on top of a prescribed atmosphere. From estimates of the fluxes and periods of acoustic waves generated in the convection zone we predict the position of the temperature minimum and the energy flux transferred to the chromosphere. The agreement between predictions and observations gives strong support to the short period acoustic heating theory of the chromosphere. A scaling law was found for radiatively damped acoustic waves. This law is used to compute acoustic frequency spectra at the base of the chromosphere.

Key words: acoustic waves — shocks — radiation damping — temperature minimum — chromospheric heating

I. Introduction

In Paper I (Ulmschneider et al., 1977) we have described our hydrodynamic code for the computation of acoustic waves and in Paper II (Kalkofen and Ulmschneider, 1977) we have discussed our treatment of radiative damping. In this third paper we employ these methods to investigate the short period heating theory of the solar atmosphere. Biermann (1946) and Schwarzschild (1948) were the first to suggest that the chromospheric temperature rise may be due to the dissipation of shocks that develop from acoustic waves generated in the solar convection zone.

The discovery of the 300 s oscillations (Leighton, 1960; Leighton et al., 1962) led to the suggestion that these oscillations could be the postulated acoustic waves (see e.g. Kuperus, 1965, 1969). However the identification of the 300 s oscillations as overstable nonradial evanescent acoustic modes of pulsations of the sun (see e.g. Deubner, 1975; Ando and Osaki, 1975) suggests that compared to the chromospheric emission roughly an order of magnitude less flux is transported by this phenomenon (Canfield and Musman, 1973, at the temperature minimum; Ulmschneider, 1976) and that shocks do not form at the temperature minimum because of the large phase shifts between velocity and brightness oscillations (Evans et al., 1963; Deubner, 1974). Thus 300 s oscillations are very likely not a significant chromospheric heating mechanism. There is even doubt whether this phenomenon constitutes a coronal heating mechanism (Ulmschneider, 1976).

A study of shock dissipation and of the chromospheric loss rate (Ulmschneider, 1970) showed that these quantities would balance at every height, if the acoustic shock waves had periods between 10 and 30 s. This was in good agreement with Stein's (1968) EE and SE acoustic spectra. Subsequent calculations (Ulmschneider, 1971a, 1971b, 1974) showed that this *short period acoustic heating theory* was able to explain the position of the temperature minimum and allowed the construction of theoretical chromospheric models. With a greatly improved treatment of the hydrodynamics and the radiative damping the present work considerably strengthens the previous conclusions. The position of the temperature minimum can be predicted with much greater accuracy than in Ulmschneider (1971b, Figures 4 and 5) and Kaplan et al. (1973, see below) and the acoustic flux at the temperature minimum may be compared with the chromospheric radiation loss. These theoretical results together with Deubner's (1975, 1976) observations of short period acoustic waves with significant power presents an impressive case for the short period acoustic heating theory of the chromosphere.

Recently Kaplan et al. (1973) have computed the height of the temperature minimum and the temperature rise in the low chromosphere using a time-independent characteristics method. Although they made many approximations in the treatment of both the wave and especially the radiative damping, using for example the diffusion approximation and an approximate form for

Send offprint requests to: P. Ulmschneider

the opacity, their conceptual approach is correct. The solution of the problem must indeed treat radiative equilibrium, radiative damping of the wave, and its mechanical dissipation in a self consistent manner. However Kaplan et al. (1973) obtained only a fair value for the height of the temperature minimum (100–300 km).

Chiuderi and Giovanardi (1975) computed the propagation and radiative damping of acoustic waves in the solar atmosphere using a linear theory. It is remarkable that their calculations, despite the great simplifications involved, show rather good agreement with our results, especially regarding the importance of radiative damping and the heights of shock formation.

In our present computation we are interested mainly in determining theoretically the location of the temperature minimum and investigating the validity of the short period acoustic heating theory. We do not try to compute from the start a completely self-consistent model atmosphere. The main difficulty with the computation of a self-consistent model atmosphere that has an accurate temperature minimum is that one needs to solve a zeroth and a first order problem simultaneously. The zeroth order problem is the construction of a radiative equilibrium atmosphere that is in reasonable agreement with the empirical models [HSRA, Gingerich et al. (1971), VAL, Vernazza et al. (1976)]. Such a computation has been performed, for example, by Kurucz (1974) who included a large number of frequency points and of continuum and line opacity sources in his nongrey, LTE calculation. The first order problem is the computation of the propagation and radiative damping of a small amplitude wave, which represents a weak perturbation of the radiative equilibrium atmosphere. In principle, such a combined first and second order computation is feasible with the methods developed in Papers I and II, but since one needs large numbers of frequency points (more than 30) to represent the line and continuum opacities the problem seems at present intractable. We decided therefore to drop the evaluation of the zeroth order problem and let the acoustic wave travel on top of an empirical model. Using a grey opacity and a small number of absorbers we find that the derivative of the net radiative flux in such an empirical model is not zero. Such a nonvanishing flux term gives rise to an entropy change, as shown in Paper II, which ultimately sets the atmosphere in motion. In order to keep the atmosphere time independent in the absence of waves we therefore have to discriminate between zeroth and first order radiation terms. Thus the radiative damping of the acoustic wave is treated as a phenomenon of first order and is computed by a perturbation method that is developed in Section II. The advantage of this procedure is obvious. The waves travel now through a realistic atmospheric model and, since the radiation damping of the wave is reasonably well approximated by taking only the most important opacity sources, the location of the temperature minimum can be predicted with greater accuracy. Section V and VI give the results of these computations and discuss the implications.

II. Perturbation Method

The transfer equation under the assumption of LTE (see Papers I and II) may be written in the Lagrange frame as

$$\mu \frac{dI_\nu(\mu,a,t)}{\varrho_0(a)\,da} = -\varkappa_\nu(a,t)\,(I_\nu(\mu,a,t)-B_\nu(a,t)), \tag{1}$$

where a is the geometrical height and ϱ_0 the density, both at time $t=0$. Integrating over angles we find for a radiative equilibrium atmosphere

$$\frac{d\pi F^0}{\varrho_0 da} = -4\pi \int_0^\infty \varkappa_\nu (J_\nu^0 - B_\nu^0)\,d\nu = 0, \tag{2}$$

where πF^0 is the total radiative flux and J_ν^0 the mean intensity. If an acoustic wave perturbs this atmosphere, an additional radiative flux πF^1 will be present. The transfer equation gives then

$$\frac{d\pi F^0}{\varrho_0 da} + \frac{d\pi F^1}{\varrho_0 da} = -4\pi \int_0^\infty (\varkappa_\nu^0 + \varkappa_\nu^1)(J_\nu^0 + J_\nu^1 - B_\nu^0 - B_\nu^1)\,d\nu. \tag{3}$$

Here the quantities have been separated into zeroth order terms, which are the values in absence of the acoustic wave, and first order terms which are due to the wave. These first order term may be assumed to be small because πF^1 is typically 1E-3 of the solar flux πF^0. Subtracting Equation (2) from (3) and neglecting terms of second order we find for the first order flux derivative

$$\frac{d\pi F^1}{\varrho_0 da} = -4\pi \int_0^\infty \varkappa_\nu^0 (J_\nu^1 - \bar{S}_\nu^1)\,d\nu. \tag{4}$$

Here J_ν^1 is computed from the first order angle dependent source function

$$S_\nu^1(\mu) = B_\nu^1 - \frac{\varkappa^1}{\varkappa^0}(I_\nu^0(\mu) - B_\nu^0). \tag{5}$$

Integrating Equation (5) over angles we find the source function $\bar{S}_\nu^1$. The radiative damping function D (see Paper II) is then given by

$$D \equiv \left.\frac{dS}{dt}\right|_{\text{Rad}} = \frac{1}{T}\frac{d\pi F^1}{\varrho_0 da} = \frac{4\pi}{T}\int_0^\infty \varkappa_\nu^0 (J_\nu^1 - \bar{S}_\nu^1)\,d\nu, \tag{6}$$

where T is the temperature and S the entropy per gram.

Table 1. Height a, temperature T, gaspressure P, Rosseland optical depth τ and the opacity $\varkappa$ of the initial model H on top of which the acoustic waves propagate. Also given are the values τ_c and $\varkappa_c$ for the Cox opacities

a (cm)	T (K)	P (dyn/cm^2)	τ	$\varkappa$ (cm^2/g)	τ_c	$\varkappa_c$ (cm^2/g)
−2.40 E 7	1.21 E 4	3.77 E 5	1.50 E 3	3.72 E 2	1.30 E 3	3.33 E 2
−1.88 E 7	1.16 E 4	3.13 E 5	7.59 E 2	2.72 E 2	6.33 E 2	2.36 E 2
−1.37 E 7	1.10 E 4	2.58 E 5	2.91 E 2	1.83 E 2	2.39 E 2	1.49 E 2
−8.57 E 6	1.00 E 4	2.10 E 5	5.61 E 1	7.85 E 1	4.65 E 1	6.55 E 1
−3.42 E 6	7.59 E 3	1.64 E 5	3.67 E 0	4.75 E 0	2.70 E 0	3.81 E 0
1.71 E 6	6.11 E 3	1.17 E 5	8.63 E−1	5.64 E−1	5.38 E−1	3.81 E−1
6.85 E 6	5.60 E 3	8.08 E 4	3.49 E−1	2.48 E−1	1.94 E−1	1.67 E−1
1.19 E 7	5.25 E 3	5.39 E 4	1.53 E−1	1.51 E−1	7.27 E−2	8.50 E−2
1.71 E 7	4.99 E 3	3.50 E 4	6.71 E−2	9.98 E−2	2.85 E−2	4.51 E−2
2.22 E 7	4.80 E 3	2.23 E 4	2.86 E−2	6.60 E−2	1.17 E−2	2.74 E−2
2.74 E 7	4.67 E 3	1.40 E 4	1.18 E−2	4.35 E−2	4.86 E−3	1.77 E−2
3.25 E 7	4.57 E 3	8.74 E 3	4.85 E−3	2.84 E−2	2.00 E−3	1.16 E−2
3.77 E 7	4.46 E 3	5.37 E 3	1.93 E−3	1.87 E−2	8.16 E−4	7.59 E−3
4.28 E 7	4.36 E 3	3.26 E 3	7.53 E−4	1.18 E−2	3.29 E−4	4.99 E−3
4.79 E 7	4.26 E 3	1.96 E 3	2.88 E−4	7.58 E−3	1.30 E−4	3.31 E−3
5.31 E 7	4.16 E 3	1.16 E 3	1.06 E−4	4.74 E−3	4.97 E−5	2.15 E−3
5.82 E 7	4.07 E 3	6.82 E 2	3.90 E−5	2.94 E−3	1.84 E−5	1.38 E−3
6.34 E 7	4.00 E 3	3.95 E 2	1.37 E−5	1.87 E−3	6.57 E−5	8.86 E−4
6.85 E 7	3.96 E 3	2.27 E 2	4.22 E−6	1.20 E−3	2.06 E−6	5.74 E−4
7.37 E 7	3.92 E 3	1.30 E 2	6.86 E−7	7.74 E−4	3.43 E−7	3.84 E−4

In order to avoid the large number of frequency points of a non-grey calculation we take the grey approximation of Equation (5), using Equation (6) in the form

$$D=\left.\frac{dS}{dt}\right|_{\text{Rad}}=\frac{4\pi\varkappa^0}{T}(J^1-\bar{S}^1), \tag{7}$$

where $\varkappa^0$ is the Rosseland mean absorption coefficient. With this the numerical method proceeds as outlined in Papers I and II.

III. Absorption Coefficient

The Rosseland mean absorption coefficients, $\varkappa(T, p)$, for normal Population I abundances have been tabulated by Kurucz (1970) for the temperature range $T=3100$ to 28000 K and the gas pressure range $\log p=-2$ to 6. This calculation involves a large number of absorbers which are listed on p. 73 of Kurucz's paper. This list of opacities in its revised form [Atlas 6, Kurucz (1975)] has been found well suited for our purposes and the main body of our work is based on this table. In order to check the uncertainty due to a different choice of the absorption coefficient we used also an extended version of the opacity tables of Cox and Stewart (1969) commonly employed in stellar evolution calculations and taken from Kippenhahn (1975). Here we have chosen the mass fractions $X=0.701$, $Y=0.278$ and $Z=0.021$ in accordance with our mean molecular weight of $\mu=1.3$. Both absorption coefficients are compared in Table 1. The Cox opacities are lower by a factor of 1.1 at large depths and 2.0 at great heights.

IV. Initial Model

In order to predict a temperature minimum for the solar atmosphere we do not use an empirical atmosphere like the HSRA (Gingerich et al., 1971) which already includes the empirical chromospheric temperature rise, but start from a model which is built under the assumption of radiative equilibrium. Comparing such a model (Kurucz, 1974) with the HSRA we derived a model which is essentially the HSRA model with a continuing temperature decrease above the height of the observed temperature minimum. This model H is given in Table 1. As an alternative we used a modified form of the recent model of Vernazza et al. (1976). This model V is shown in Table 2. Admittedly there is some arbitrariness in this procedure as Non-LTE effects (Cayrel effect) are neglected in the radiative equilibrium atmosphere of Kurucz (1974). However there is no model presently available that includes both lines and Non-LTE effects.

V. Results

a) Heights of Shock Formation

Assuming that the temperature minimum lies roughly in the first quarter of the region between formation and full development of the shock we find from Figures 4 and 5 of Ulmschneider (1971b) that the theoretical temperature minimum must lie within about one quarter scale height above the point of shock formation. Naturally the exact position of both shock formation and temperature minimum can only be found by a detailed computation taking into account Non-LTE effects (Cayrel effect).

Table 2. Height a, temperature T, gaspressure P, Rosseland optical depth τ and the opacity $\varkappa$ of the initial model V on top of which the acoustic waves propagate

a (cm)	T (K)	P (dyn/cm^2)	τ	$\varkappa$ (cm^2/g)
−2.40 E 7	1.21 E 4	3.77 E 5	1.50 E 3	3.72 E 2
−1.88 E 7	1.16 E 4	3.13 E 5	7.59 E 2	2.71 E 2
−1.37 E 7	1.10 E 4	2.58 E 5	2.91 E 2	1.83 E 2
−8.57 E 6	1.00 E 4	2.10 E 5	5.61 E 1	7.85 E 1
−3.42 E 6	7.59 E 3	1.64 E 5	3.72 E 0	4.74 E 0
1.71 E 6	6.12 E 3	1.17 E 5	9.07 E−1	5.74 E−1
6.85 E 6	5.69 E 3	8.12 E 4	3.61 E−1	2.72 E−1
1.20 E 7	5.30 E 3	5.44 E 4	1.57 E−1	1.54 E−1
1.71 E 7	5.01 E 3	3.55 E 4	6.85 E−2	1.01 E−1
2.22 E 7	4.81 E 3	2.26 E 4	2.91 E−2	6.69 E−2
2.74 E 7	4.66 E 3	1.42 E 4	1.19 E−2	4.38 E−2
3.25 E 7	4.53 E 3	8.84 E 3	4.75 E−3	2.83 E−2
3.77 E 7	4.38 E 3	5.39 E 3	1.81 E−3	1.79 E−2
4.80 E 7	4.11 E 3	1.91 E 3	2.33 E−4	6.65 E−3
5.31 E 7	3.97 E 3	1.11 E 3	7.78 E−5	3.92 E−3
5.82 E 7	3.83 E 3	6.33 E 2	2.44 E−5	2.17 E−3
6.34 E 7	3.69 E 3	3.53 E 2	7.09 E−6	1.18 E−3
6.85 E 7	3.55 E 3	1.92 E 2	1.79 E−6	6.28 E−4
7.37 E 7	3.41 E 3	1.02 E 2	2.41 E−7	3.16 E−4

However we feel that in spite of these difficulties our computed heights of shock formation give some indication of the position of a theoretical temperature minimum. We have performed a number of calculations in which we excited the atmosphere given by Table 1 at the bottom by a sinusoidally oscillating piston, the motion of which is determined by specified values of the acoustic period and initial flux (see Paper I). In order to keep the effect of the transients small we always started with an expansion wave.

Figure 1 shows the Eulerian height of shock formation as a function of wave period with the initial flux as parameter. The heights of the HSRA and VAL temperature minima are indicated. Heavy lines show computation for model H. Thin lines indicate results for model V. Also given is the height of shock formation for the calculations with no radiative damping, taken from Paper I. This shows (assuming one quarter scale height between shock formation and temperature minimum) that for initial fluxes between 3 and 6 E7 erg/cm^2 s the empirical HSRA and VAL temperature minima are reproduced to about half a scale height if the wave period is in the range 25 to 45 s.

Because the shock position cannot be found to an accuracy of better than two times the height distance between two adjacent grid points the shock formation heights have an error $\pm$ 10 km as indicated by an error bar in Figure 1.

Figure 1 clearly shows the influence of two main effects on the shock formation. The first is that long period waves produce shocks at greater heights because the peak of the compression region in such waves has to travel an increased distance in order to meet the expansion valley. This effect has already been described by

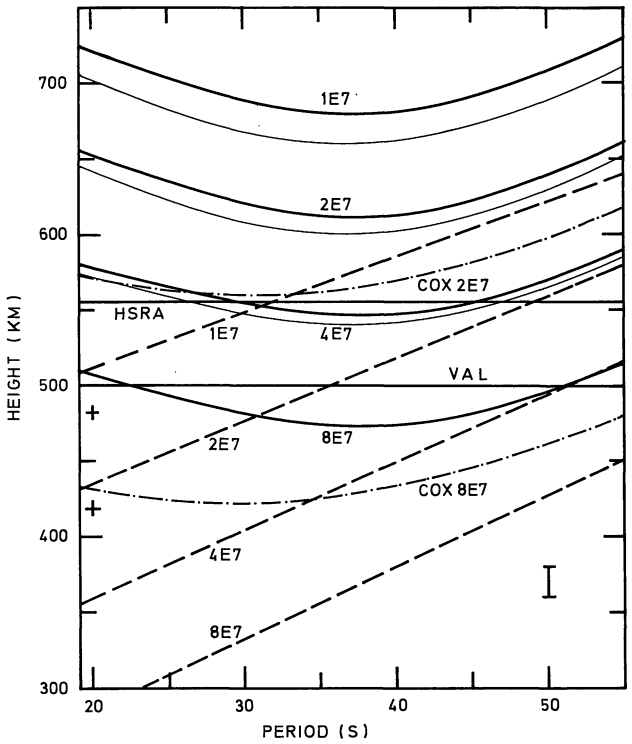

Fig. 1. Shock heights (temperature minima) as function of wave period with initial flux as parameter for model H (drawn) and model V (thin). Shock heights of waves without radiative damping are shown dashed. HSRA and VAL indicate the empirical temperature minima. COX labels calculations with Cox opacities. + indicates calculations with finer grid size

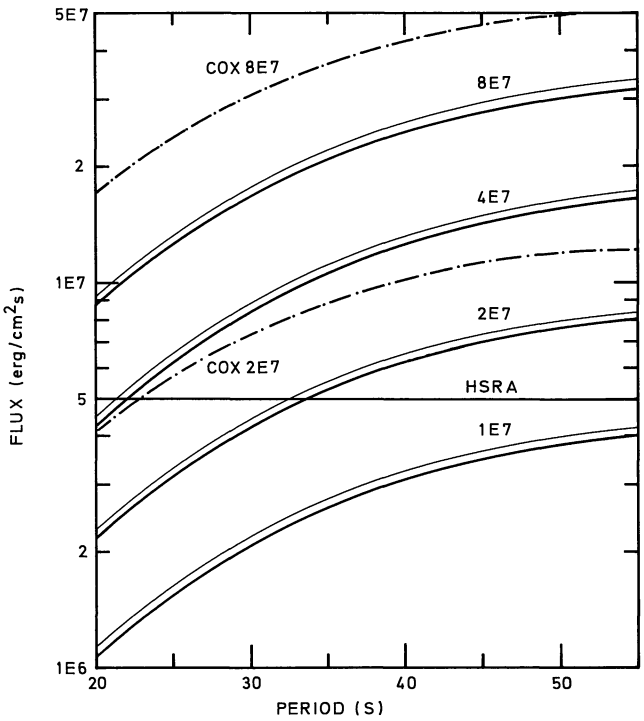

Fig. 2. Acoustic flux at shock formation (drawn) as function of period and initial flux for model H (drawn) and model V (thin). HSRA indicates the empirical chromospheric radiation flux. COX labels calculations with Cox opacities

Ulmschneider (1971a) and is demonstrated by the shock formation heights without radiation. The second effect is due to radiative damping which acts most strongly at small period (Oster, 1957; Spiegel, 1957). The reason for this is that radiative damping at large optical depth is proportional to the second derivative of the mean intensity. This curvature is larger for small periods. At small optical depth the optical distance between high and low temperature areas of the wave is proportional to the wavelength. Thus radiative damping preferentially weakens short period waves and increases the heights of shock formation. It is seen that a factor of two decrease in wave flux increases the shock height by about 0.7 scale heights.

The influence of the choice of the initial model is shown in Figure 1. Since the upper photospheric temperatures in model *V* are smaller than those in model *H*, the scale heights in model *V* are reduced and the acoustic waves develop into shocks earlier. Because of the increasing temperature difference between models *H* and *V* at great heights, the differences in the heights of shock formation increase with altitude for similar initial flux and period.

b) Acoustic Flux at Shock Formation

Figure 2 shows the acoustic flux at the height of shock formation as function of period and initial flux. Heavy lines are fluxes computed for model *H*, thin lines are fluxes for model *V*. Also indicated is the empirical chromospheric radiation flux of 5.0 E6 erg/cm^2 which is due to H^- (Athay, 1970; Ulmschneider, 1974) and the Ca^+ H+K and Mg^+ $h+k$ lines (Ayres, 1975, p. 158). It is seen that waves with periods of less than 40 s and initial fluxes between 1E7 and 5E7 erg/cm^2 s carry enough energy at shock formation to balance the empirical chromospheric radiation loss. These calculations show somewhat surprisingly, that the effect of radiative damping is not as severe as was estimated (Ulmschneider, 1971b) from approximate calculations, and that a much larger fraction of the initial wave energy reaches the chromosphere. This seems to rule out the large acoustic fluxes of between 5.5E7 and 1.0 E8 erg/cm^2 s computed by Stein (1968) which were obtained from a solar convection zone calculation using a rather large ratio of mixing length to pressure scale height, $\alpha=2.0$. Scaling Stein's result to values between $\alpha=1.1$ to 1.3 that are currently accepted (Christensen-Dalsgaard and Gough, 1976) and using an $\alpha^{2.8}$ dependence of the acoustic flux (Renzini et al., 1977) we find fluxes between 1.0 E7 and 3.0 E7 erg/cm^2 s, which are in good agreement with the initial fluxes which we found above. The influence of the choice of the initial atmospheric model on the final acoustic flux is minor, as seen in Figure 2 because radiative damping occurs primarily at optical depths between $\tau=0.1$ and 10, where the temperature difference between models *H* and *V* is small.

c) Spatial Variation of Velocity, Pressure and Temperature

In Figure 3 we show the velocity u, the perturbations of the temperature T, and the pressure P, as well as the radiative damping function D as function of height and optical depth.

The perturbations of T and P travel on top of the undisturbed atmosphere given by Table 1. The wave has a period of 20 s and an initial flux of $\pi F_I=2.0$ E7 erg/cm^2 s and is shown at time 98 s, after the first disturbance enters from the bottom with an expansion. This initial disturbance has just reached the right hand side of the figure. Because of numerical effects inherent in the use of a transmitting boundary condition at a fixed height, as described in Paper I, the initial onset of the expansion wave is spread over a few grid points toward greater heights. Similar calculations for periods of 35 and 50 s are shown in Figures 4 and 5. The waves suffer significant radiative damping at optical depths from $\tau=10$ to 0.05. This is indicated by the outward decrease of the u amplitudes. In this region an adiabatic wave would grow considerably because of the density decrease. After the radiative damping zone the waves grow rapidly because of energy conservation. In the optically thin region $\tau\leqq 0.01$ radiative damping indicated by the damping function, D, is shown to have the opposite sign of the T oscillation. This is understood as the basis of the optically thin approximation. A high temperature region rapidly looses energy by radiation, leading to a high rate of entropy decrease. The relative error using the optically thin approximation is about 10% at $\tau=0.01$ and about 1E-4 at the upper boundary. At large optical depth radiative damping becomes rapidly small. Here the diffusion approximation is good down to $\tau=1$.

Figures 3–5 show also calculations with different initial flux $\pi F_I=8.0$ E7 erg/cm^2 s. The results appear simply scaled by the square root of the ratio of the initial fluxes. Small differences in the calculations are explained (Ulmschneider, 1971b) by the increased distortion of the large amplitude waves which is accompanied by growth due to energy conservation. This scaling law, valid for radiatively damped acoustic waves, is familiar from our calculations of adiabatic waves in Paper I. For the radiative damping function D the scaling property is due to the linear dependence of D on the density and temperature perturbations in Equation (7).

d) Time Behaviour of the Waves

The time behaviour of the waves of Figures 3–5 is similar to an adiabatic calculation. However due to radiation the temperature, although following the general pattern of the velocity behaviour, shows large changes in amplitude and departs from the sinusoidal wave form in space. Consider the transmission of a compression peak through the radiative damping zone. We show in Figures 6–8 temperature T, velocity u, entropy S and the radiative

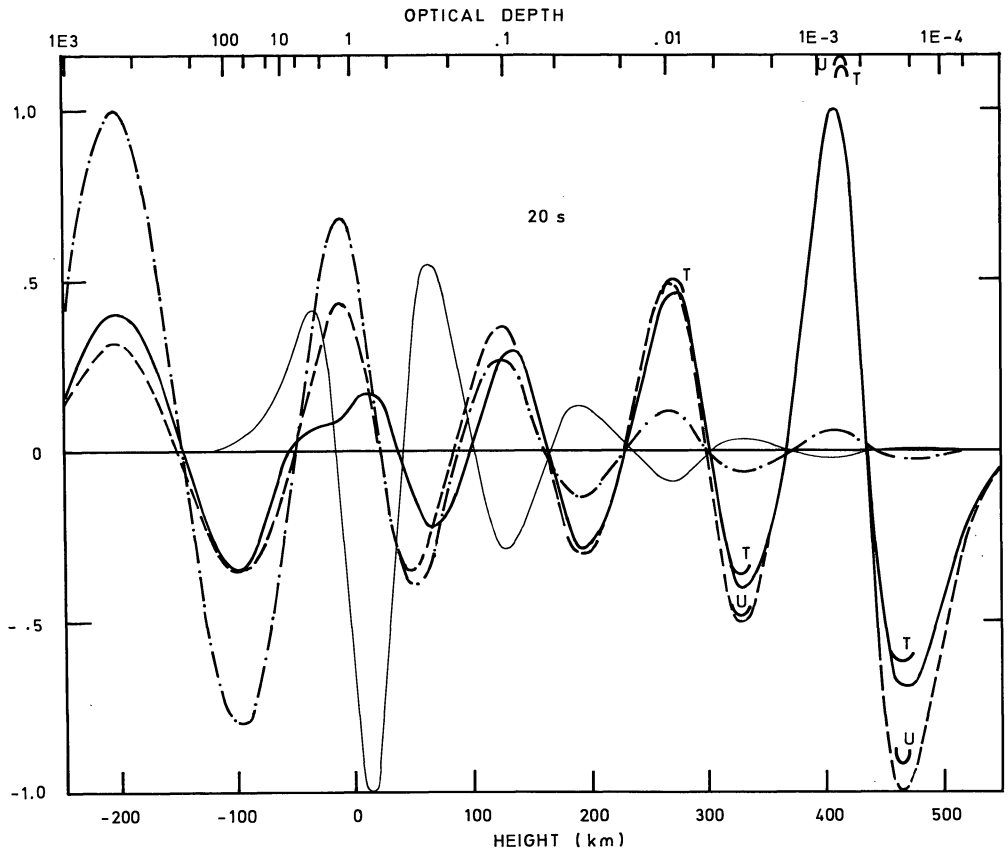

Fig. 3. Acoustic wave of period 20 s and initial flux $\pi F_I = 2\,\mathrm{E}\,7$ erg/cm^2 s at time $t = 98$ s. Both geometrical height and optical depth are given. Gas velocity u (dashed), temperature perturbation $T' = T - T_0$ (drawn), pressure perturbation $p' = p - p_0$ ($- \cdot \cdot -$) and radiative damping function D (lightly drawn) are given. The ordinates have to be multiplied by the values in brackets: u (2.88 E 4 cm/s), T' (1.41 E 2 K), p' (4.19 E 3 dyn/cm^2), D (3.55 E 5 erg/g s K). Small arcs indicate an identical calculation except $\pi F_I = 8\,\mathrm{E}\,7$ erg/cm^2 s. Here the ordinates are larger by a factor of 2

damping function D at three neighbouring times. Due to Equation (7), and the strong temperature dependence of $\varkappa^1$, radiative damping is primarily a function of temperature. In an adiabatic wave of the same period, velocity and temperature perturbations are nearly in phase. Thus we picture the velocity to indicate the shape and position of the temperature profile in the absence of radiative damping. Figure 6 shows that near $\tau = 1$ the temperature is much reduced because of radiative damping. The emitted photons which give rise to a negative peak of the D-function, are seen to be absorbed at lower and at higher optical depths (positive peaks of the D-function), heating up the medium there. In Figure 7 the increasing compression (see Figures 3–5, note that pressure is in phase with velocity) near $\tau = 0.5$ tries to raise the temperature near the front of the velocity peak while lowering it at the back. Damping makes the forward part of the wave the main photon source. At the back of the wave the temperature is decreased because of expansion in spite of photon absorption. Figure 8 shows the situation where the compression peak has left the radiative damping zone while the subsequent expansion wave cools the medium strongly. This results in a large influx of photons (D-function peak at $\tau = 0.7$) to heat up the expansion wave. The situation is now the opposite to Figure 6 and further time development is explained by using similar arguments on the next expansion peak. Note how the large phase lag between temperature and velocity of the compression peak decreases with distance from $\tau = 0.1$. This is due to the fact that the less radiative damping occurs the more the temperature follows the adiabatic behaviour. Generally because the node after the compression peak (Fig. 6, $h = 120$ km) moves into a region where strong radiative losses have occured, in the p-T diagram an adiabat of lower entropy and consequently a lower temperature prevail. Thus the temperature is always shifted forward in phase, relative to the velocity.

e) Scaling Property of the Acoustic Flux

Comparing in Figure 2 acoustic fluxes at fixed periods we note that the final flux is proportional to the initial flux. The ratio of initial to final flux, being a constant for a given period, is shown in Table 3 as function of period.

This important property of the flux of radiatively damped acoustic waves is due to the scaling behaviour described in Section Vc). It was shown that for two calculations at identical times, for example the velocities,

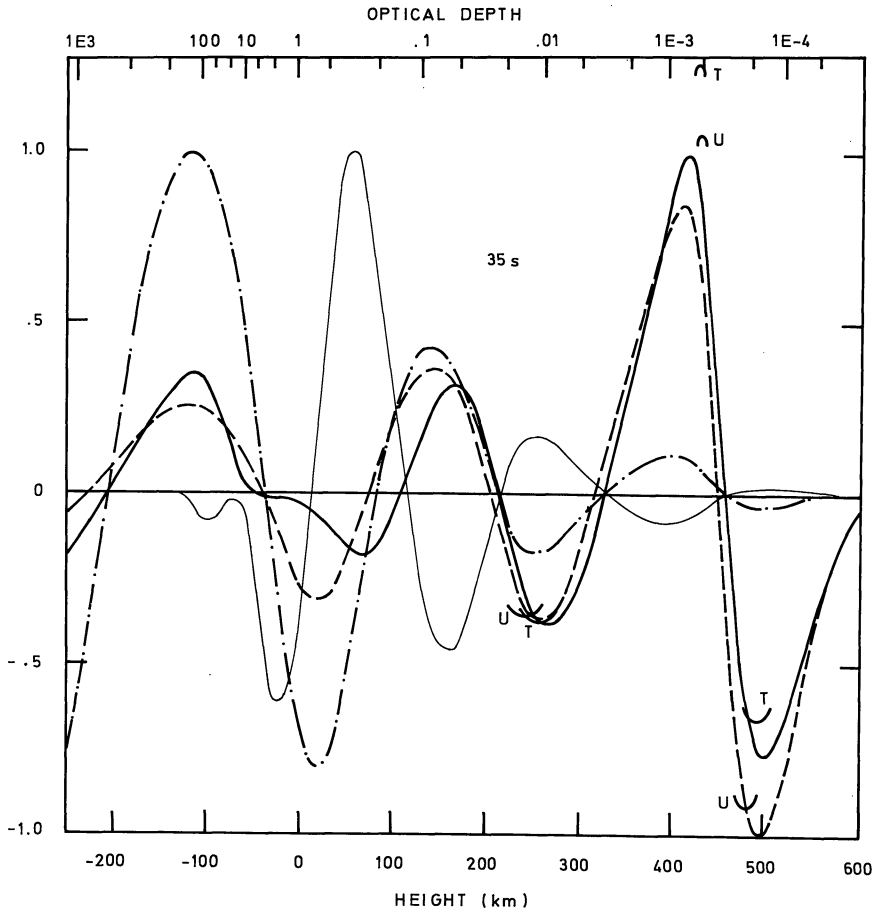

Fig. 4. Acoustic wave of period 35 s with $\pi F_1 = 2\,\mathrm{E}\,7\,\mathrm{erg/cm^2}$ at $t = 107$ s, similar to Figure 3. The ordinates are u(4.97 E 7), T' =(2.14 Es), p' (3.88 E 3), D (2.57 E 5). The ordinates for the calculation with πF_1 $= 8\,\mathrm{E}\,7\,\mathrm{erg/cm^2\,s}$ are larger by a factor of 2

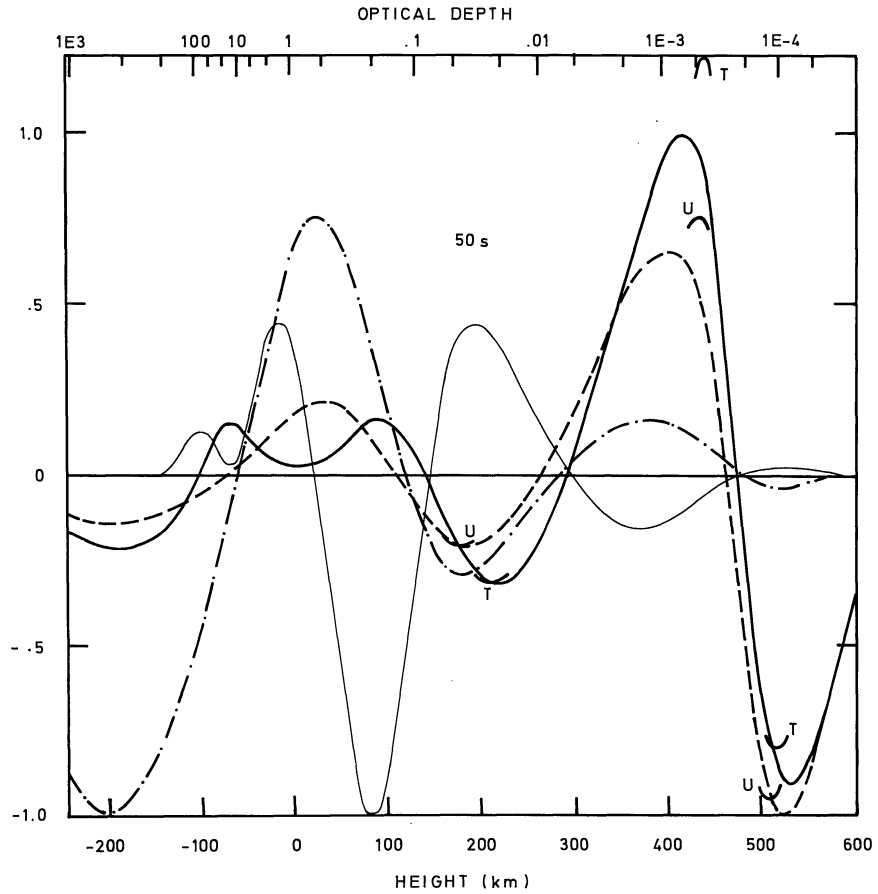

Fig. 5. Acoustic wave of period 50 s with πF_I $= 2\,\mathrm{E}\,7\,\mathrm{erg/cm^2\,s}$ at $t = 115$ s, similar to Figure 3. The ordinates are u (6.58 E 4), T' (2.28 E 2), p' (3.40 E 3), D (1.70 E 5). The ordinates for the calculation with πF_I $= 8\,\mathrm{E}\,7\,\mathrm{erg/cm^2\,s}$ are larger by a factor of 2

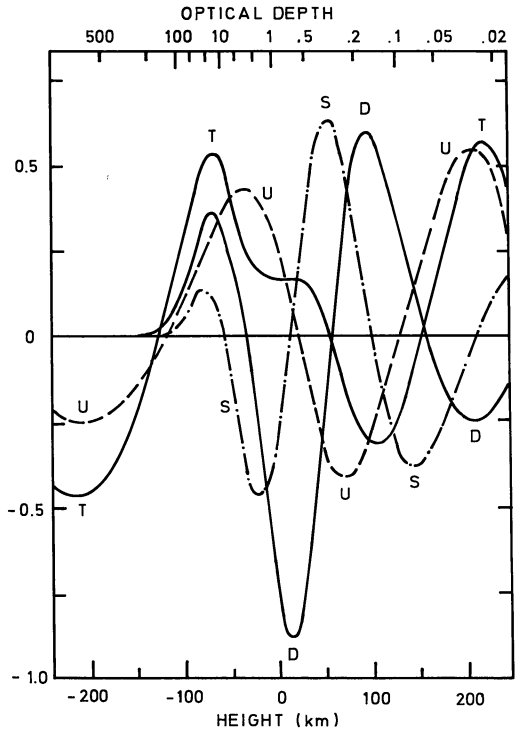

Fig. 6. Acoustic wave with period 35 s and initial flux $\pi F_I = 2\,\mathrm{E}\,7$ erg/cm^2 s at time 81 s. U, T', S, D label gas velocity, temperature-, entropy perturbation and radiative damping function. The ordinates have to be multiplied by the values in brackets, u (3.5 E 4 cm/s), T (1.5 E 2 K), S (2.0 E 6 erg/gK), D (3.0 E 5 erg/gsK)

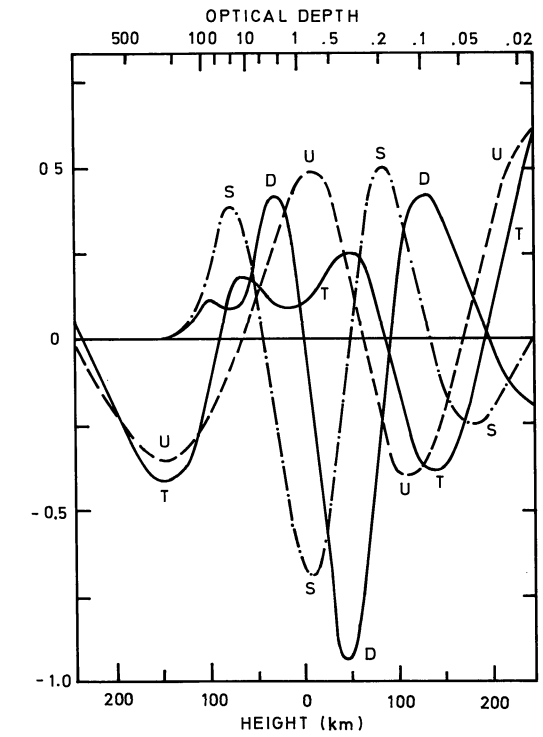

Fig. 7. Same as Figure 6 but at time $t = 87$ s

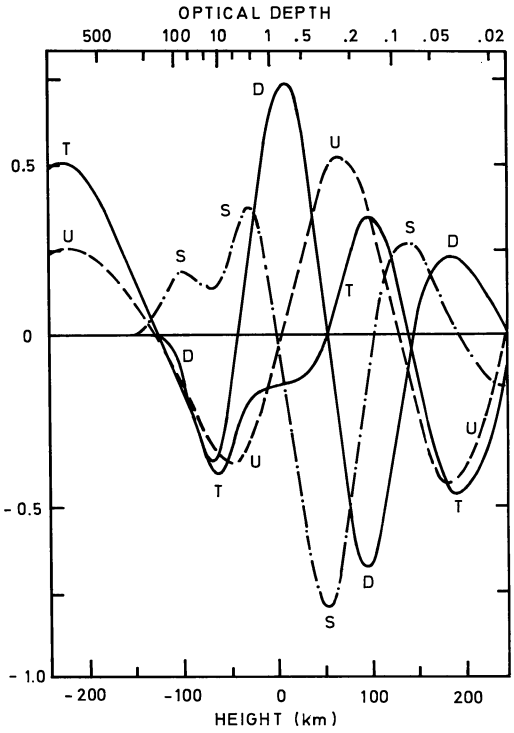

Fig. 8. Same as Figure 6 but at time $t = 97$ s

Table 3. Ratio of initial to final flux for acoustic waves of various periods. The values depend weakly on the models chosen but strongly on the opacities assumed. Kur labels Kurucz (1975) opacities, Cox labels Cox and Stewart (1969) opacities

Model	Opacity	Period (s)						
		20	25	30	35	40	45	50
H	Kur	9.4	6.3	4.7	3.8	3.2	2.9	2.6
V	Kur	8.9	6.0	4.4	3.6	3.0	2.7	2.5
H	Cox	4.6			2.1			1.7

u_1, u_2, and the pressure perturbations, p_1', p_2', scale like the square root of the ratio of the initial fluxes, πF_{I1}, πF_{I2},

$$\frac{u_2}{u_1} \approx \frac{p_2'}{p_1'} \approx \left(\frac{\pi F_{I2}}{\pi F_{I1}}\right)^{1/2}. \tag{8}$$

As the final fluxes, πF_{F1} and πF_{F2}, are proportional to $p_1' u_1$ and $p_2' u_2$ respectively we have

$$\frac{\pi F_{F2}}{\pi F_{F1}} \approx \frac{\pi F_{I2}}{\pi F_{I1}}, \tag{9}$$

where, as shown in Table 3, the slope of the linear relationship between πF_{F2} and πF_{I2} depends on the wave period.

f) Validity of the Perturbation Approach

In applying our perturbation approach in the derivation of Equation (7), we have assumed that the first order

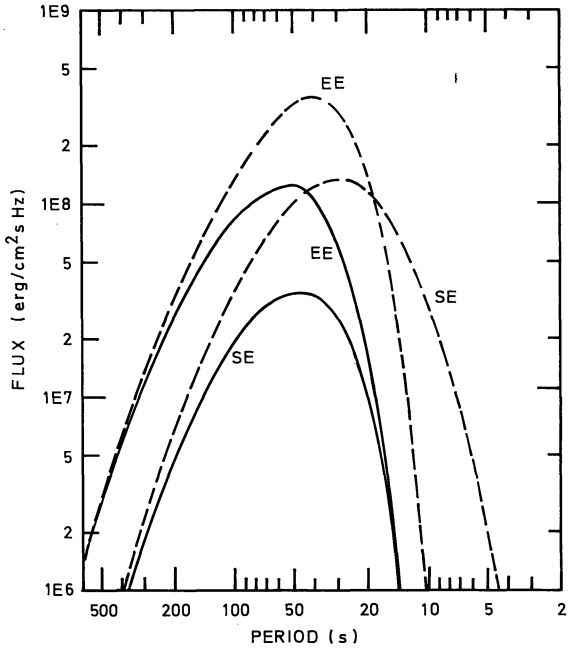

Fig. 9. Acoustic frequency spectra (drawn) at the temperature minimum after passage of the radiation damping zone. The spectra generated in the convection zone (Stein, 1968) are shown dashed. Here $\alpha = 2.0$

terms at the right hand side of Equation (3) are small compared to the zeroth order terms. A comparison of different terms for the wave of $\pi F_I = 2.0$ E7 erg/cm^2 s shown in Figure 3 reveals that $\varkappa^1$ is at most 4% of $\varkappa^0$ and that J^1, B^1, S^1 are at most 3% of J^0.

g) Influence of the Choice of Opacities

To estimate how much our results depend on the choice of opacities, we have computed a small number of cases with the Cox opacities described in Section III. The resulting acoustic fluxes are shown in Figure 2 and in Table 3. It is seen that the effect of radiative damping on the waves is considerably decreased. The reason for this is the smaller magnitude of the Cox opacities for $\tau < 1$. Because of reduced radiative damping the shock formation heights are decreased as seen in Figure 1.

h) Influence of the Grid Size

As the grid size is most critical for short period waves we recomputed the case of the 20 s wave with the number of points per wavelength increased by a factor of 1.4. Both for the Kurucz and the Cox opacities we found a less than 7% change in the final flux. The finer grid spacing decreases the height of shock formation somewhat for a wave of $P = 20$ s and $\pi F_I = 8$E7 erg/cm^2 s (+sign in Fig. 1). This error is comparable to the error of the shock finding. We thus concluded that the grid size taken was sufficiently small and that our results are independent of the choice of the grid.

i) Comparison with the Work of Chiuderi and Giovanardi

It is interesting to compare our results with those of Chiuderi and Giovanardi (1975) who used a linear time independent theory. Our general finding that radiative damping is relatively inefficient is also demonstrated in their Figure 1 and Table 1. Our scaling law [Eq. (9)] is seen to apply in their Table 1. For instance for the 31.4 s waves they find a factor of 2.6 which is in good agreement with our results of Table 3. However it appears that their linear approach overestimates the radiative damping for long period waves. Comparing the shock heights of their 31.4 s waves with ours we find good agreement except for the wave with smallest flux. This may be due to the fact that we use a modified HSRA while their case was computed on basis of the observed HSRA, in which the rising temperature increases the height of shock formation. Thus restricting their results to the domain of short period waves we find a remarkably good agreement between our and Chiuderi and Giovanardi's (1975) work.

VI. Discussion

a) The Chromospheric Heating Mechanism

In this paragraph we want to summarize arguments which can be made in favour of the short period acoustic heating mechanism.

1. In any discussion of the heating of the chromosphere one has to start with the observational confirmation of short period acoustic waves in the solar atmosphere (Deubner, 1975, 1976) with fluxes of several times 10^8 erg/cm^2 s. Note that because of phase shifts between pressure and velocity oscillations (Ulmschneider, 1976), Deubner's values are upper estimates of the actual acoustic flux. It would be hard to explain why a considerable fraction of the energy of these freely propagating (because of their small period) waves should not reach the chromosphere.

2. The Lighthill-Proudman mechanism of acoustic sound generation, when applied to the solar convection zone predicts (Stein, 1968) acoustic spectra peaking at periods between 25 and 40 s and fluxes of the order of 2.5 to 4.5 E7 erg/cm^2 s when scaled to $\alpha = 1.5$ (see Fig. 9).

3. We have seen in Section Va) that the heights of shock formation agree within about a scale height with the position of the empirical temperature minimum if the initial acoustic fluxes are in the range 3 to 6E7 erg/cm^2 s and the acoustic periods are between 25 and 45 s. Larger periods would lead invariably to a considerable increase in the height of shock formation [see also Fig. 5 of Paper I]. Thus short period waves are able to explain the low height of the empirical temperature minimum.

4. We found in Section Vb) that the acoustic flux at shock formation agrees well with the empirical chromospheric radiation loss if the initial acoustic fluxes are

Table 4. As function of the parameter α (mixing length/pressure scale height), theoretical values of the acoustic flux πF_I, acoustic period P_{Max}, shock formation height h_0 as well as chromospheric radiation flux πF_0 are given. A comparison with empirical values is indicated. The empirical radiation flux is given by Ayres (1975)

α	πF_I erg/cm^2 s	P_{Max} (s)	h_0 (km)	πF_0 erg/cm^2 s
1.00	1.6 E 7	27.5	650	3.2 E 6
1.25	3.0 E 7	26.0	590	5.0 E 6
1.50	5.1 E 7	24.5	540	7.2 E 6
Empirical		HSRA	550	5.0 E 6
Empirical		VAL	500	

between 2 and 6E7 erg/cm^2 s and the periods are less than 35 s.

5. Short period waves explain the empirical gradient of the emission rate in the chromosphere (Ulmschneider, 1970, 1974). Shock waves of long periods will have increasing dissipation with height as the wave grows in a medium of decreasing density. Thus only short period waves, having decreasing dissipation with height, are able to balance the empirically found decreasing emission rate of the chromosphere.

To summarize we feel that all these arguments taken together argue fairly convincingly for the short period acoustic waves as the main chromospheric heating mechanism. There are still difficulties, for instance, how to explain the apparent increased emission in the chromospheric network. One possible explanation could be a more efficient generation of acoustic waves in presence of strong magnetic fields (see e.g. Kulsrud, 1955). Another explanation (Uchida, 1963) could be a delay of shock formation by the magnetic field resulting in a greater shock dissipation at larger altitudes. A third possibility could be a transfer of acoustic energy into the region enclosed by the magnetic field.

b) A Theoretical Temperature Minimum

To construct a theoretical temperature minimum we have computed total acoustic fluxes πF_I using the Lighthill (1952) and Proudman (1952) theory employing the envelope part of a stellar structure program (Renzini et al., 1977). We replace the acoustic flux spectrum by a single vertically propagating plane wave of period $P = P_{\text{Max}}$, where P_{Max} is the maximum of the acoustic spectrum. P_{Max} is given (Stein and Leibacher, 1974) approximately by

$$P_{\text{Max}} = \frac{1}{10} P_A = \frac{1}{10} \frac{4\pi c}{\gamma g}, \tag{12}$$

where c is the sound velocity at maximum sound generation and P_A the acoustic cut off period. The theoretical temperature minimum is found at the height of shock formation h_0. The acoustic flux, πF_0, at this height should be able to balance the chromospheric radiation loss. Results are seen in Table 4.

c) Acoustic Flux Spectra at the Temperature Minimum

The scaling law of radiatively damped acoustic waves described in Section V lets us predict the shape of the acoustic frequency spectrum at the temperature minimum. Because the choice of the initial model between the HSRA or the model of Vernazza et al. (1976) does not influence significantly the magnitude of radiation damping (see Fig. 2), Table 3 may be used to compute the effect of radiative damping on the acoustic frequency spectra of Stein (1968). The result is shown in Figure 9. It is seen that large period waves suffer little radiation damping and consequently are readily available to the heating of the upper chromosphere and lower corona. Note that Figure 9 is computed using $\alpha = 2.0$. For other values the fluxes must be scaled like $\alpha^{2.8}$.

Acknowledgement. It is a pleasure fur us to acknowledge stimulating discussions with Dr. L. Cram of the Fraunhofer Institute, Freiburg and with Drs. F. Meyer and H. U. Schmidt of the Max-Planck-Institut, Munich.

References

Ando, H., Osaki, Y.: 1975, *Publ. Astron. Soc. Japan* **27**, 581
Athay, R. G.: 1970, *Astrophys. J.* **161**, 713
Ayres, T. R.: 1975, Ph.D. Thesis, Univ. of Colorado, Boulder
Biermann, L.: 1946, *Naturwiss.* **33**, 118
Canfield, R. C., Musman, S.: 1973, *Astrophys. J.* **184**, L 131
Chiuderi, C., Giovanardi, C.: 1975, *Solar Phys.* **41**, 35
Christensen-Dalsgaard, J., Gough, D. O.: 1976, *Nature* **259**, 89
Cox, A. N., Stewart, J. N.: 1969, *Astrophys. J. Suppl.* **19**, 243
Deubner, F.: 1974, *Solar Phys.* **39**, 31
Deubner, F.: 1975, Nice meeting on Physics of Motions in Stellar Atmospheres, International Colloquium of the CNRS, ed. R. Cayrel and M. Steinberg, 1976
Deubner, F.: 1976, *Astron. Astrophys.* **51**, 189
Evans, J. W., Michard, R., Servajean, R.: 1963, *Ann. Astrophys.* **26**, 368
Gingerich, O., Noyes, R. W., Kalkofen, W., Cuny, Y.: 1971, *Solar Phys.* **18**, 347
Kalkofen, W., Ulmschneider, P.: 1977, *Astron. Astrophys.* (in press)
Kaplan, S. A., Ostrovskii, L. A., Petrukhin, N. S., Fridman, V. E.: 1973, *Soviet Astron.* **16**, 1013
Kippenhahn, R.: 1975, private communication
Kulsrud, R. M.: 1955, *Astrophys. J.* **121**, 461
Kuperus, M.: 1965, *Rech. Astron. Observ. Utrecht* **17**, 1
Kuperus, M.: 1969, *Space Sci. Rev.* **9**, 713
Kurucz, R.: 1970, SAO *Spec. Rep.* 309
Kurucz, R.: 1974, *Solar Phys.* **34**, 17
Kurucz, R.: 1975, private communication
Leighton, R. B.: 1960, Proc. IAU Symp. **12**, 321 (*Nuovo Cimento Suppl.* **22**)
Leighton, R. B., Noyes, R. W., Simon, G. W.: 1962, *Astrophys. J.* **135**, 474
Lighthill, M. J.: 1952, *Proc. Roy. Soc. London* A**211**, 564
Oster, L.: 1957, *Z. Astrophys.* **44**, 26
Proudman, I.: 1952, *Proc. Roy. Soc. London* A**214**, 119

Renzini, A., Cacciari, C., Ulmschneider, P., Schmitz, F.: 1977, to be published
Schwarzschild, M.: 1948, *Astrophys. J.* **107**, 1
Spiegel, E. A.: 1957, *Astrophys. J.* **126**, 202
Stein, R.: 1968, *Astrophys. J.* **154**, 297
Stein, R., Leibacher, J.: 1974, *Ann. Rev. Astron. Astrophys.* **12**, 407
Uchida, Y.: 1963, *Publ. Astron. Soc. Japan* **15**, 376
Ulmschneider, P.: 1970, *Solar Phys.* **12**, 403
Ulmschneider, P.: 1971a, *Astron. Astrophys.* **12**, 297
Ulmschneider, P.: 1971b, *Astron. Astrophys.* **14**, 275
Ulmschneider, P.: 1974, *Solar Phys.* **39**, 327
Ulmschneider, P.: 1976, *Solar Phys.* **49**, 249
Ulmschneider, P., Kalkofen, W., Nowak, T., Bohn, H. U.: 1976, *Astron. Astrophys.* **54**, 61
Vernazza, J. E., Avrett, E. H., Loeser, R.: 1976. *Astrophys. J. Suppl.* **30**, 1
Vitense, E.: 1953, *Z. Astrophys.* **32**, 135